Matrix-Isolation ESR Studies of the Various Isotopomers of the CH_3Zn and ZnH Radicals: Comparisons with ab Initio Theoretical Calculations†

Allan J. McKinley* and Emmanuel Karakyriakos

Department of Chemistry, The University of Western Australia, Nedlands, Perth, Western Australia 6907

Lon B. Knight, Jr.,* Robert Babb, and Aaron Williams

Chemistry Department, Furman University, Greenville, South Carolina 29613

Received: September 20, 1999; In Final Form: December 10, 1999

The $^{12}CH_3Zn$, $^{12}CH_3{}^{67}Zn$, $^{13}CH_3Zn$, $^{13}CH_3{}^{67}Zn$, $^{13}CD_3{}^{67}Zn$, and $^{13}CD_3Zn$ radicals have been isolated in an inert neon matrix at 4.3 K. Their electronic structure has been probed for the first time using matrix-isolation electron spin resonance spectroscopy (MI-ESR). These radicals were generated by the reaction of laser-ablated zinc metal with the appropriate methyl precursor. The magnetic parameters (MHz) were determined to be $g_\perp = 1.9835(4)$, $A_\perp(H) = 14(1)$, $A_\perp(D) = 2.2(4)$, $A_\perp(^{13}C) = 166(3)$, and $A_\perp(^{67}Zn) = 547(1)$. Estimates were derived for $A_{||}(^{13}C) = 211(50)$ and $A_{||}(^{67}Zn) = 608(5)$. The ^{67}ZnH radical was also generated by the reaction of laser-ablated zinc metal and hydrogen gas and studied for the first time by MI-ESR after isolation in solid neon matrixes at 4 K. The values of the ^{67}ZnH magnetic parameters (MHz) were determined to be $g_\perp = 1.9841(3)$, $g_{||} = 1.9990(5)$, $A_\perp(H) = 505(1)$, $A_{||}(H) = 503(1)$, $A_\perp(^{67}Zn) = 615(1)$, and $A_{||}(^{67}Zn) = 660(1)$. Earlier argon MI-ESR studies produced ZnH by conventional high-temperature methods and determined only the hydrogen hyperfine interaction and the molecular g tensor. Hartree−Fock single- and double-excitation configuration interaction (HFSDCI) and multireference single- and double-excitation configuration interaction (MRSDCI) ab initio calculations of the magnetic hyperfine interactions in the CH_3Zn and ZnH radicals were performed. The $A_{iso}(^{67}Zn)$ and the $A_{dip}(^{67}Zn)$ values calculated for both radicals were within 10% of the experimental observations. However, the calculated $A_{iso}(^{13}C)$ values for the CH_3Zn radical were low by about 50%, and the calculated $A_{iso}(H)$ value for ZnH was low by 60%. Density functional theory (DFT) yielded A_{iso} values for H and ^{13}C in much closer agreement with experiment. A comparison is presented between the ESR results for the CH_3Zn and ZnH radicals and their cadmium analogues, which have been investigated previously by MI-ESR.

I. Introduction

Several isotopomers of the CH_3Zn radical and the ^{67}ZnH radical have been isolated in inert, solid neon matrices and studied for the first time by electron spin resonance spectroscopy (ESR). The CH_3Zn radicals were formed by the reaction of laser-ablated zinc metal with various methyl precursors, including $(^{12}CH_3)_3Al$, $^{13}CD_3I$, $^{13}CH_3I$, and $(^{13}CH_3)_2{}^{12}CO$. The values of $g_\perp$, $A_\perp(H)$, $A_\perp(D)$, $A_\perp(^{13}C)$, and $A_\perp(^{67}Zn)$ were determined directly from the experimental spectra, and estimates for $A_{||}(^{13}C)$ and $A_{||}(^{67}Zn)$ were derived from higher-order influences on the observed perpendicular line positions. The ^{67}ZnH radical was formed by the reaction of laser-ablated zinc metal and hydrogen gas. These results represent the first experimental determination of the zinc hyperfine interaction for "simple" radicals isolated in an inert, gaslike environment and the first ESR study of the CH_3Zn radical. The ESR spectrum of the ZnH radical isolated in an argon matrix was reported earlier, but detection of the ^{67}Zn ($I = {}^5/_2$; 4.1% natural abundance) hyperfine structure was not achieved.[1] A major focus of this report will be a comparison of the observed and calculated magnetic parameters for CH_3Zn and ZnH. Such a comparison will help to establish the degree of electronic-structure change in a "simple" metal compound when the H ligand is replaced with the CH_3 ligand.

As part of this study, the structure of the CH_3Zn radical has been evaluated from ab initio calculations. The geometry was also compared with that obtained from earlier calculations[2−5] and with the very recent experimental geometry derived from resonant-enhanced multiphoton ionization (REMPI) spectroscopy and from zero kinetic energy pulsed-field ionization (ZEKE-PFI) spectroscopy by Barckholtz and co-workers.[5] Configuration interaction (CI) and density functional theory (DFT) ab initio calculations of the hyperfine coupling constants have been performed for the CH_3Zn and ZnH radicals, and these results were compared with the experimental matrix ESR results. The electronic structures derived from these MI-ESR experiments for the CH_3Zn and ZnH radicals can also be compared with those derived from MI-ESR studies of their cadmium analogues, CdH, CH_3Cd, and CdOH.[1,6,7]

The CH_3Zn radical is formed as an intermediate in the photodissociation of $(CH_3)_2Zn$ to zinc atoms and two methyl radicals.[8−10] Knowledge of the bonding and electronic structure of the CH_3Zn radical intermediate is of considerable interest, given the use of $(CH_3)_2Zn$ in the electronics industry as a source of zinc metal, through the metal organic chemical vapor deposition (MOCVD) process,[11] for the manufacture of zinc-containing wide-gap type-II/VI semiconductor materials such as ZnSe.[12] Zinc is an important biological trace metal that is present in many enzymes, including alcohol dehydrogenase,

† Part of the special issue "Marilyn Jacox Festschrift".

10.1021/jp993358u CCC: $19.00
Published on Web 02/10/2000

carbonic anhydrase, DNA and RNA polymerase, carboxypeptidase, and thermolysin.[13] Although these species do not involve a direct zinc−carbon or zinc−hydrogen bond, information on the simple radical species presented here will provide useful benchmarks for other zinc-containing radicals. There have been very few reports of zinc hyperfine data because of the low natural abundance of ^{67}Zn and its high nuclear spin. To our knowledge, the only ESR studies that have reported ^{67}Zn hyperfine-structure values involve either defects in a crystal of a zinc compound or chelated zinc ions in solution.[14,15] Species containing metal−carbon and metal−hydrogen bonds are implicated in important transition-metal-catalyzed reactions and are thought to be intermediates in C−H and C−C activation.[16] Dialkylzinc compounds also have applications as reagents in organic synthesis.[17] The UV absorption spectrum of the CH_3-Zn radical was first reported by Young and co-workers in 1973.[8] Several laser-induced fluorescence studies of this radical have been conducted in the gas phase and have determined vibrational frequencies and the electronic configuration of the CH_3Zn radical.[18−22] In recent experiments, Barckholtz and co-workers[5] have derived high-resolution, "experimental" molecular-orbital diagrams for both CH_3Zn and CH_3Mg. However, the nuclear hyperfine interactions of the CH_3Zn radical have not been observed. Several matrix-isolation IR studies involving zinc molecules have been conducted. Hauge and co-workers[23] have reported $ZnCH_2$ and CH_3ZnH. Ault and Bai have reported argon-matrix studies of the reaction of $(CH_3)_2Zn$ with group-V and group-VI hydrides,[24] with group-V and group-VI alkyls,[25] and with CH_3OH and CH_3SH.[26] Greene and co-workers[27] have reported the reaction of excited metal atoms with methane to generate species of the type CH_3MH, where M = Zn, Cd, or Hg in argon matrixes; the CH_3ZnH species produced in this study was found to be photostable and did not yield the CH_3Zn radical when irradiated with the broad-band output of a 500-W medium-pressure Hg lamp. Greene and co-workers[28] have also reported the reaction of excited metal atoms to form species of the type MH_2 (M = Zn or Cd) isolated in argon matrixes and have performed ab initio calculations on these species; in these experiments, the ZnH radical was observed. Bracken and co-workers[29,30] found no evidence for the CH_3Zn radical from irradiation (down to 155 nm) of $(CH_3)_2Zn$ isolated in an argon matrix at 12 K.

Recently, we have studied the CH_3Cd radical and its isotopomers isolated in argon and neon matrixes using ESR spectroscopy.[6] Related small radicals, such as CH_3Pd,[31] CH_2-Cu,[32] CH_3CuH,[33] CH_3GaH,[34] and CH_3AlH,[35] have been investigated by ESR when trapped in low-temperature matrices. Recent high-resolution gas-phase studies have investigated species that include CH_3Ba,[36] CH_3Ca,[37−39] CH_3Mg,[40,41] CH_3-Na,[42] CH_3Sr,[43,44] and CH_3Cd[22,45] and its cation.[46]

The ZnH radical has been studied by optical spectroscopy for many years,[47] and various absorption features have been observed in stellar spectra.[48,49] Recent studies have included laser-induced fluorescence measurements,[50,51] diode laser vibrational spectroscopy,[52,53] and Fourier transform emission spectroscopy.[54] The gas-phase hydrogen hyperfine data for the ZnH radical have been reported for the $A^2\Pi$ state[50] and recently for the $X^2\Sigma^+(v=0)$ state of the ZnH and ZnD radicals.[55,56] The activation of H−H, Si−H, and C−H bonds by the nsnp excited states of the Zn atom has been reviewed recently.[57] Theoretical investigations of ZnH have included studies of low-lying excited states[58] and of the reaction dynamics of the system $Zn(^3P) + H_2/D_2/HD$.[59]

II. Experimental Section

The neon-matrix ESR experiments involving the CH_3Zn radical were performed at The University of Western Australia (UWA); the ZnH work was conducted at Furman University. During these initial ZnH experiments, unassigned background radical ESR absorptions were observed that were later shown to be those of CH_3Zn. As detailed accounts of the apparatus and experimental procedures employed in both laboratories have already been reported,[6,60] only a brief description of the important details of the experimental procedures will be given here.

The CH_3Zn radical was generated by reacting zinc vapor with neon-matrix gas (Spectra Gases; research grade) doped with a methyl precursor. The methyl precursors, $(^{12}CH_3)_3Al$ (Aldrich), $^{13}CH_3I$ (Aldrich, 99 at. % ^{13}C), $^{13}CD_3I$ (Aldrich, 99 at. % ^{13}C and D), and $(^{13}CH_3)_2{}^{12}CO$ (Sigma, 98 at. % ^{13}C), were used as received, after being degassed by several freeze−pump−thaw cycles. The zinc metal vapor was formed by laser ablation of a high-purity zinc metal target (Alfa, 99.998% metal purity) with the frequency-doubled output (532 nm) of a Nd:YAG laser (Surelite I), operating at 10 Hz and a pulse energy of approximately 10 mJ. The beam was focused to a tight spot (7.5-cm focal-length lens) on the zinc target and was continuously rastered over the metal surface during matrix deposition. The matrix was deposited onto an oxygen-free, high-conductivity copper deposition target that was maintained at 4.3 K by a continuous-flow liquid-helium cryostat (Cryo Industries of America RC110). Deposition times varied between 30 and 90 min, depending on the ESR signal strength required for the particular experiment. Typical background pressures, before cooling the cryostat, ranged from 5×10^{-8} to 1×10^{-7} Torr. The methyl precursors were introduced as dopants in the neon-matrix gas at a flow rate of 6−9 standard cubic centimeters per minute (sccm) into the ablation chamber near the zinc vapor plume. These mixtures were made in a glass preparation line using pressure ratio measurements (MKS Baratron). The prepared mixtures had methyl precursor concentrations of between 200 and 300 ppm. The ESR spectra were recorded on a Bruker ESP300E spectrometer with a DM4116 cavity.

Generation of the ^{67}ZnH radical was accomplished using a laser-vaporization method similar to that described above. The H_2 (or D_2) gas in its pure state was passed directly over the spot on the zinc metal target that was undergoing laser ablation. The radicals generated in this way were trapped in neon on a copper flat, which was located at a distance of approximately 5 cm from the zinc target. The ZnH radicals were created directly in the laser-induced metal−gas reaction region, and/or they were created from co-deposition reactions of Zn atoms (or ions) with H atoms during neon-matrix condensation. The amount of H_2-(g) introduced was approximately 0.1% of the amount of neon-matrix gas employed, which was introduced at a rate of 4 sccm for a 1-h deposition. The copper deposition surface was maintained at approximately 4.4 K by a closed-cycle helium refrigerator (APD model HS 304). The spectrometer employed for the ZnH experiments was a Varian E-109 using the standard X-band microwave cavity and operating in the TE_{102} mode with 100-kHz modulation.

Because the ^{67}Zn hyperfine interaction was observed to be large, spectral analysis was conducted through an exact diagonalization of the spin Hamiltonian using the program GEN developed by Knight and co-workers at Furman University.[60,61] The spin Hamiltonian employed was

$$\hat{H} = \beta_e \bar{B}\cdot\hat{g}\cdot\bar{S} + \sum_i (\bar{I}^i\cdot\hat{A}^i\cdot\bar{S} - \hat{g}_I{}^i\beta_n\bar{B}\cdot\bar{I}^i)$$

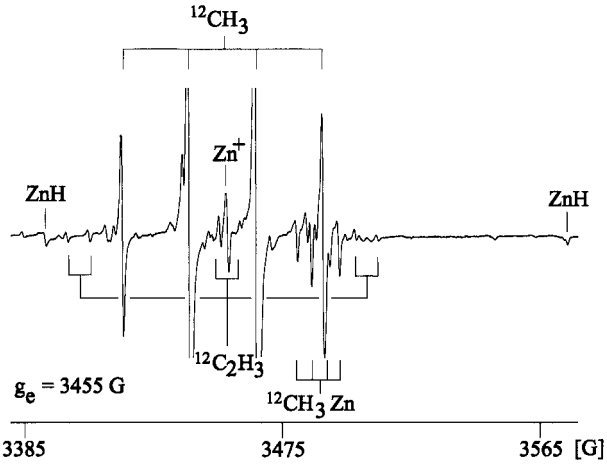

Figure 1. The center field region of the ESR spectrum shows the $^{12}CH_3$-Zn radical isolated in a neon matrix at 4.3 K. The spectrum was recorded with a microwave power of 1 mW and a microwave frequency of 9682.75(1) MHz. The $^{12}CH_3Zn$ radical was generated from the reaction of laser-ablated zinc metal with $(^{12}CH_3)_3Al$. The $^{12}CH_3Zn$ radical spectrum consists of a quartet of lines (the H:$M_J = -^1/_2$ line is obscured by the H:$M_J = -^3/_2$ line of the $^{12}CH_3$ radical) all with a "phase-down" pattern. Only the perpendicular transitions of the radical are observed. The parallel transitions are weaker and are not observed in this spectrum. The ESR peaks of the $^{12}CH_3$, ZnH, and $^{12}C_2H_3$ radicals and the Zn^+ cations are also labeled.

where all symbols have their usual meanings, and where the sum over *i* includes hyperfine contributions from all magnetic nuclei.[62] Inclusion of a term to account for quadrupole effects involving the ^{67}Zn nucleus was not found to be necessary in order to obtain good agreement between the experimental and calculated values of the ESR line positions. This fact is not surprising, given the large ^{67}Zn isotropic hyperfine interaction. Ab initio calculations employed the MELDF suite of programs and the Gaussian 94 package.[63,64]

III. Results

A. The CH_3Zn Radical. Natural zinc metal consists of five different isotopes, ^{64}Zn (48.9%), ^{66}Zn (27.8%), ^{67}Zn (4.1%), ^{68}Zn (18.6%), and ^{70}Zn (0.6%). Of these isotopes, only ^{67}Zn ($I = ^5/_2$, $\mu = 0.87524$) has a non-zero nuclear spin and can produce a nuclear hyperfine interaction. For simplicity, ESR signals arising from those isotopomers with $I = 0$ for Zn will be designated "Zn", with no specific isotopic label.

The ESR spectrum assigned to the $^{12}CH_3Zn$ radical, formed from the reaction of laser-ablated zinc metal and $(^{12}CH_3)_3Al$ and isolated in a neon matrix at 4.3 K, is shown in Figure 1. Hydrogen ($I = ^1/_2$) is the only nucleus in the $^{12}CH_3Zn$ radical that has a non-zero nuclear spin; therefore, the expected signal is a 1:3:3:1 quartet from the three equivalent hydrogen atoms. The higher-field line of the central pair (H:$M_J = -^1/_2$) is obscured by the highest-field line (H:$M_J = -^3/_2$) of the $^{12}CH_3$ radical. This quartet is located upfield of g_e, and the observed intensity ratio is not quite 1:3:3:1. Also, additional lines that are spaced between the expected quartet lines are observed. When the sample is annealed to 8.5 K, these additional lines disappear, and the intensity ratio of the quartet approaches the expected 1:3:3:1. We have reported an analogous behavior for the CH_3Cd radical, which we attributed to tunneling rotation about the C_3 axis at low temperature.[6] The "phase-down" line shape suggests that the radical exhibits axial symmetry and that these are the perpendicular peaks. The weaker parallel lines, which are difficult to detect because they would be expected to occur in the congested region closer to g_e, could not be observed.

TABLE 1: Magnetic Parameters (MHz) of the Isotopomers of the CH_3Zn Radical

	$g_\perp$[a]	$A_\perp$[b]	$A_\parallel$[b]	A_{iso}[b,c]	A_{dip}[b,c]
H[d]	1.9835(4)	−14(1)	−	−14(1)	−
D[d]	1.9835(4)	−2.2(4)	−	−2.2(4)	−
^{13}C	1.9835(4)	166(3)	211(50)	182(19)	14(22)
^{67}Zn	1.9835(4)	547(1)	608(5)	569(3)	20(4)
	1.9835(4)[e]	545(1)[e]	607(5)[e]	567(3)[e]	20(4)[e]

[a] The value of $g_\parallel$ is assumed to be 2.0. [b] Experimental uncertainties in the parameters are based on the change required to shift any one of the simulated line positions outside the uncertainty bounds of the experimental line positions. For $A_\parallel(^{13}C)$, the effect on the calculated line shape was also employed. See text. [c] Values for A_{iso} and A_{dip} were calculated from standard expressions and include a correction for $L\cdot I$ effects. These experiments cannot determine the signs of A_{iso} and A_{dip}; the signs given are those that show the closest agreement with theoretical values. [d] The value of A_{dip} for hydrogen is small; hence, A_{iso} is assumed to be equal to $A_\perp$. [e] Alternate trapping-site parameters. See text.

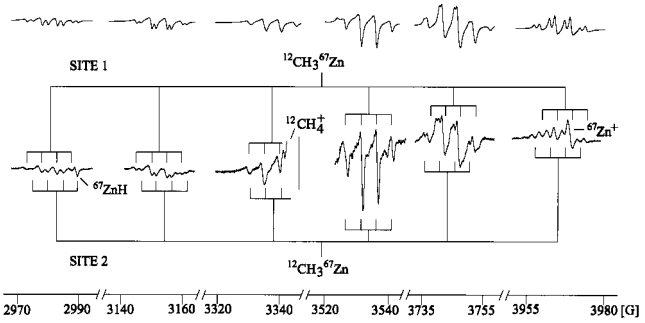

Figure 2. The lower trace shows the complete experimental ESR spectrum of the $^{12}CH_3{}^{67}Zn$ radical in neon at 9.0 K. The spectra were recorded with a microwave power of 1 mW and a microwave frequency of 9686.10(50) MHz. The methyl source used was $(^{12}CH_3)_3Al$. The $^{12}CH_3{}^{67}Zn$ radical occupies two slightly nonequivalent sites in the matrix, denoted "Site 1" and "Site 2". Also labeled are the peaks of the ^{67}ZnH, $^{12}CH_4^+$, and $^{67}Zn^+$ radicals that occur in this field region. The upper trace shows the simulated ESR spectrum for the $^{12}CH_3{}^{67}Zn$ radical, using the appropriate magnetic parameters from Table 1.

Calculated line positions agreed with the observed line positions within the experimental uncertainty of ±0.4 G, using an exact diagonalization analysis of the spin Hamiltonian and the magnetic parameters given in Table 1.

The yield of $^{12}CH_3Zn$ radical in these experiments was substantially higher than that of $^{12}CH_3Cd$, which was generated in our earlier experiments under analogous experimental conditions.[6] The ESR signals from the $^{12}CH_3$ radical and the Zn^+ ion were observed, as well as weak signals due to the $^{12}C_2H_3$,[65] $^{12}CH_4^+$,[66] and ZnH radicals.[1] Impurity radicals such as $H^{12}CO$,[62] H_2O^+,[67] and N[62] atoms were also observed in most spectra.

Confirmation of the assignment of the quartet pattern shown in Figure 1 to the $^{12}CH_3Zn$ radical was obtained by detecting the ^{67}Zn ($I = ^5/_2$) hyperfine lines due to the $^{12}CH_3{}^{67}Zn$ radical and the ^{13}C hyperfine lines due to the $^{13}CH_3Zn$ radical. The expected ESR spectrum of the $^{12}CH_3{}^{67}Zn$ radical should consist of six widely spaced quartets. The quartet line spacing in each of these ^{67}Zn hyperfine transitions should be the same as that in the $^{12}CH_3Zn$ radical. Although *g* and *A* tensor anisotropy will influence the intensity of the ^{67}Zn sextet components, they should be approximately 0.7% as intense as the $^{12}CH_3Zn$ absorption. The observed spectrum of the $^{12}CH_3{}^{67}Zn$ radical in a neon matrix is shown as the lower trace in Figure 2. Because of the particular combination of *g* and *A* tensor anisotropy, the low-field lines tended to be weaker than the high-field lines. The $^{12}CH_3$ quartet of the ^{67}Zn:$M_I = -^1/_2$ line also shows at 4.3

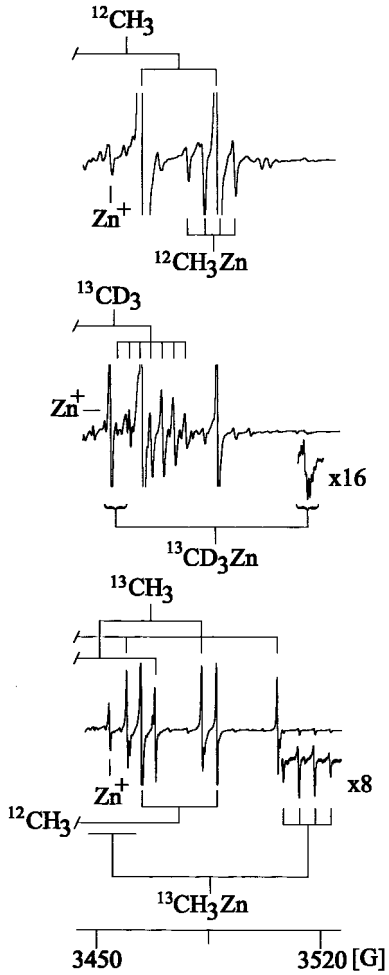

Figure 3. ESR spectra of various isotopomers of the CH_3Zn radical isolated in a neon matrix. The top trace shows the ESR spectrum of the $^{12}CH_3Zn$ radical recorded at 8.5 K with a microwave power of 1 mW and a microwave frequency of 9682.97(1) MHz. The radical was generated from the reaction of laser-ablated zinc metal with $(^{12}CH_3)_3Al$. The center trace shows the ESR spectrum of the $^{13}CD_3Zn$ radical with an offset trace magnified 16 times. The spectrum was recorded at 9.5 K with a microwave power of 0.1 mW and a microwave frequency of 9679.35(1) MHz. The lower-field septet is obscured by other peaks. The methyl source used was $^{13}CD_3I$. The bottom trace shows the ESR spectrum of the $^{13}CH_3Zn$ radical with an offset trace magnified 8 times. The spectrum was recorded at 9.5 K with a microwave power of 0.1 mW and a microwave frequency of 9677.42(1) MHz. The lower-field quartet is obscured by other peaks. The methyl source used was $(^{13}CH_3)_2CO$. Background radicals $^{12}CH_3$, $^{13}CH_3$, $^{13}CD_3$, and Zn^+ are labeled.

K the same additional lines associated with tunneling that were discussed above for the $^{12}CH_3Zn$ radical. Only the perpendicular transitions ($\theta = 90°$, where θ is the angle between the applied magnetic field and the molecular symmetry axis) were observed in these matrix samples. The ^{67}Zn hyperfine lines were split into closely spaced pairs of quartets at low and high fields. This splitting was attributed to the $^{12}CH_3{}^{67}Zn$ radicals occupying two slightly different sites in the neon matrix, with each site having slightly different magnetic parameters. (A similar site behavior was seen for the $^{12}CH_3{}^{111}Cd$ and $^{12}CH_3{}^{113}Cd$ radicals in neon matrixes.[6]) The spectrum of each site is denoted as "Site 1" or "Site 2" in Figure 2. The top trace of Figure 2 shows the simulated ESR spectrum, calculated by averaging over all orientations of the radical with an exact diagonalization analysis of the spin Hamiltonian using the magnetic parameters listed in Table 1. Each site was simulated independently, and then, the two simulations were summed to produce the spectrum that is shown. The two sites were found to be present in a ratio of approximately 1:1.

These experiments alone cannot determine the signs of the ^{67}Zn coupling constants; the signs given are based on the theoretical predictions (vide infra). Because the much weaker parallel lines were not observed in these experiments, the $A_{||}$ value for ^{67}Zn was estimated from higher-order shifts in the perpendicular line positions, using the perpendicular g value derived from analysis of the $^{12}CH_3Zn$ radical.

The ESR spectrum of $^{13}CH_3Zn$, formed by reacting $(^{13}CH_3)_2{}^{12}CO$ with laser-ablated zinc, is shown in the lower trace of Figure 3 for a neon matrix at 9.5 K. The top trace of Figure 3 shows the ESR spectrum (perpendicular lines only) of the $^{12}CH_3Zn$ radical recorded at 8.5 K in neon for comparison. At this higher temperature, the quartet intensities are closer to the expected 1:3:3:1 ratio for the three equivalent hydrogen atoms, and the tunneling peaks are no longer present. The low-field lines of the ^{13}C doublet occur in the g_e region of the spectrum and are partially obscured by the Zn^+ absorption and the triplet due to N atoms. The high-field quartet of the ^{13}C doublet is shown magnified ($\times 8$) in the lower offset trace, and the quartet splitting exactly matches that shown for the $^{12}CH_3Zn$ radical in the top trace. In all experiments conducted with ^{13}C-labeled methyl precursors, small yields of the ^{12}C isotopomer were also observed. The ^{12}C methyl source was presumably derived from decomposition of the diffusion pump oil. Also labeled in the lower trace of Figure 3 are the signals due to Zn^+ ions and $^{12}CH_3$ and $^{13}CH_3$ radicals.

For a final spectral confirmation, the $^{13}CD_3Zn$ radical was generated by reaction of $^{13}CD_3I$ with laser-ablated zinc metal. The center trace of Figure 3 shows the ESR spectrum of the $^{13}CD_3Zn$ radical in a neon matrix recorded at 9.5 K. A new, partially unresolved multiplet, shown magnified $\times 16$ in the offset trace, is located exactly at the center of the high-field quartet seen for the $^{13}CH_3Zn$ radical. This septet is due to the three equivalent deuterium nuclei ($I = 1$). Again, the low-field septet is not observed, as it falls in the g_e region of the spectrum and is obscured by the Zn^+ signal and the peaks due to N atoms. Also labeled on the center trace of Figure 3 are the high-field septet of the $^{13}CD_3$ radical and the line for the Zn^+ ion. The ratio of the observed hyperfine splitting of deuterium to that of hydrogen agrees with the expected value.

The ^{13}C splitting was observed on the more intense, unobscured lines of the ^{67}Zn sextet. The ESR spectrum of the ^{67}Zn: $M_I = -3/2$ group for the $^{12}CH_3{}^{67}Zn$ radical is shown in trace (a) of Figure 4, that for the $^{13}CD_3{}^{67}Zn$ radical in trace (b), and that for the $^{13}CH_3{}^{67}Zn$ radical in trace (c). Inspection of the ESR spectrum of the $^{13}CD_3{}^{67}Zn$ radical clearly shows the ^{13}C doublet (which is denoted $^{13}CD_3{}^{67}Zn$) positioned about the quartet from the residual $^{12}CH_3{}^{67}Zn$ radical absorption in this magnetic-field region. This spectrum is recorded under high-modulation conditions to optimize the signal-to-noise ratio, and consequently, the deuterium splitting is not resolved. The high-field hydrogen line occurs near 3700 G and lowers the baseline in the vicinity of the low-field ^{13}C component. However, it can be seen that the phase of the low-field line of the ^{13}C doublet is between "phase down" and symmetrical and that the phase of the high-field line of the ^{13}C doublet is "phase up". The assignment of these peaks to the $^{13}CD_3{}^{67}Zn$ radical was confirmed when the $^{13}CH_3{}^{67}Zn$ radical was formed and the two expected quartets replaced the two unresolved peaks, as shown in trace (c) of Figure 4.

With a methyl source of $^{13}CH_3I$, we observed a much larger production of trapped hydrogen atoms. The effect on the slope

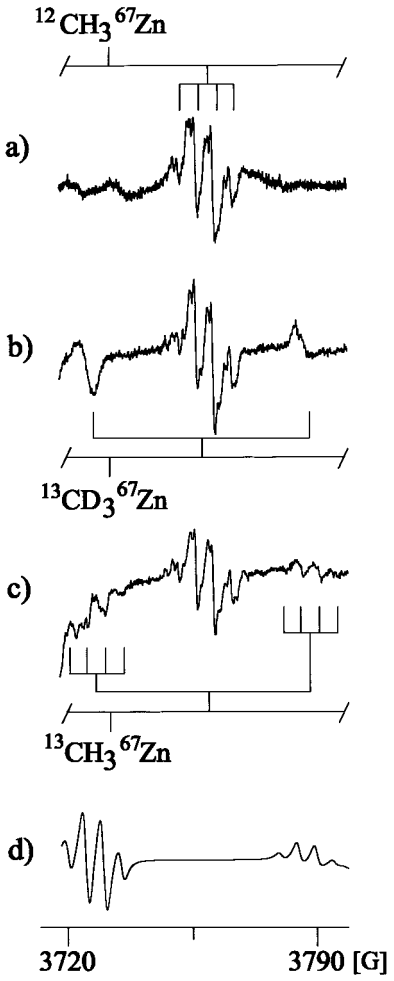

Figure 4. ESR spectra of ^{67}Zn:$M_I = -3/2$ lines of various isotopomers of the $^{12}CH_3{}^{67}Zn$ radical in neon. Trace (a) shows the ESR spectrum of the $^{12}CH_3{}^{67}Zn$ radical (^{67}Zn:$M_I = -3/2$) recorded at 9.0 K with a microwave power of 1 mW and a microwave frequency of 9685.74(1) MHz. The methyl source used was $(^{12}CH_3)_3Al$. Trace (b) shows the ESR spectrum of the $^{13}CD_3{}^{67}Zn$ radical (^{67}Zn:$M_I = -3/2$) recorded at 9.5 K with a microwave power of 1 mW and a microwave frequency of 9725.69(1) MHz. The methyl source used was $^{13}CD_3I$. Trace (c) shows the ESR spectrum of the $^{13}CH_3{}^{67}Zn$ radical (^{67}Zn:$M_I = -3/2$) recorded at 9.5 K with a microwave power of 1 mW and a microwave frequency of 9724.13(4) MHz. The methyl source used was $^{13}CH_3I$. Trace (d) shows the simulated ESR spectrum for the $^{13}CH_3{}^{67}Zn$ radical (^{67}Zn:$M_I = -3/2$) that was constructed using the appropriate magnetic parameters from Table 1.

of the baseline was minimized by subtracting a simulated first-derivative Gaussian line from this spectrum in order to reduce the baseline slope. The peaks of the low- and high-field quartets also show a change in phase that is analogous to the change shown in the $^{13}CD_3{}^{67}Zn$ radical spectrum. As anticipated, the centers of both quartets are located at the same field position as the centers of the two unresolved $^{13}CD_3{}^{67}Zn$ radical septets.

A series of simulations was conducted to determine the hyperfine coupling constants for the ^{13}C nucleus. Because we had only observed the perpendicular transitions, only $A_\perp(^{13}C)$ could be determined directly from these experiments, and this value is given in Table 1. However, the line shape and the positions of the perpendicular lines did show a dependence on the value of $A_\parallel(^{13}C)$ that was used in the simulated spectrum, allowing an estimated value of 211(50) MHz to be determined for $A_\parallel(^{13}C)$. These ESR experiments alone could not determine the signs of the hyperfine coupling constants, and the signs reported in Table 1 were chosen to yield the closest agreement with the theoretical calculations. Trace (d) of Figure 4 shows the simulated spectrum for the $^{13}CH_3{}^{67}Zn$ radical in this field region calculated using exact diagonalization of the spin Hamiltonian and the parameters given in Table 1.

TABLE 2: Comparison of the Experimental and Theoretical Magnetic Parameters (MHz) of the ZnH Radical

	^{67}Zn		H	
	A_{iso}	A_{dip}	A_{iso}	A_{dip}
experimental[a]	630(1)	15(1)	503(1) (501.9)[b]	−1(1) (−0.094)[b]
theoretical[c]				
HFSDCI[d,e]	610	17	178	[−1.2, −1.2, 2.4]
MRSDCI[f]	598	17	199	[−0.83, −0.83, 1.66]
DFT[g]	552	−	609	−

[a] This work; laser-ablation generation, neon matrix. For ^{67}Zn, $A_\parallel$ = 660(1) and $A_\perp$ = 615(1) MHz. For H, $A_\parallel$ = 503(1) and $A_\perp$ = 505(1) MHz. The measured g values are $g_\perp$ = 1.9841(3) and $g_\parallel$ = 1.9990(5). [b] High-resolution gas-phase measurements of the H hyperfine interaction, refs 55 and 56. Metal hyperfine interaction not yet measured in gas phase. [c] This work. The uncontracted basis sets used were the Wachters basis set for zinc with the recommended two additional p functions (14s 11p 5d) and the uncontracted Dunning DZP set for hydrogen (4s 1p).[68,69] [d] All single excitations from the Hartree−Fock solution and those double excitations that exceeded an energy threshold of 5×10^{-7} hartree were retained in the CI calculation. [e] The HFSDCI calculation included 68 275 spin-adapted configurations, had a sum of squares of the coefficients in the reference space of 0.96, and had a total CI energy of −1779.0704 hartree. [f] The MRSDCI calculation used 40 reference configurations chosen on the basis of their CI coefficient from the HFSDCI calculation. The MRSDCI calculation included 238 919 spin-adapted configurations, had a sum of squares of the coefficients in the reference space of 0.97, and had a total CI energy of −1779.0804 hartree. All single excitations from the reference space and those double excitations that exceeded an energy threshold of 5×10^{-7} hartree were retained in the CI calculation. [g] DFT calculation used the same basis set as above with geometry optimized to a Zn−H distance of 1.5947 Å.

B. The ZnH Radical. The ESR spectrum of the ZnH radical isolated in neon matrices and formed from the reaction of laser-ablated zinc metal is very similar to that reported earlier, for which the ZnH radical was generated from the reaction of thermally generated zinc vapor and hydrogen atoms and was isolated in an argon matrix.[1] The experimental ESR line positions for ZnH and ^{67}ZnH agree with those calculated from an exact diagonalization analysis of the spin Hamiltonian using the magnetic parameters listed in Table 2. Recent gas-phase measurements of the hydrogen hyperfine interaction are also given in Table 2.[55,56] The neon-matrix value of A_{iso} = 503(1) MHz for H shows close agreement with the gas-phase result of 501.9 MHz.

The ESR spectrum of ^{67}ZnH (Figure 5) consists of a ^{67}Zn ($I = 5/2$) sextet of hydrogen doublets from the H ($I = 1/2$) nucleus. As discussed above, these ^{67}Zn ESR lines are only about 0.7% of the intensity of the ZnH lines, and only the lines corresponding to perpendicular orientations of ^{67}ZnH were observed, except for two of the more intense parallel features. The intense H-atom doublet absorption is shown by dashed lines in Figure 5. The low-field hydrogen line partially obscures the high-field line of the ^{67}Zn:$M_I = 3/2$ doublet. A simulation of the overall spectrum obtained from an exact diagonalization analysis of the spin Hamiltonian using the parameters given in Table 2 is shown in the lower half of Figure 5. The value of $A_\parallel$ was estimated by using the shifts in the perpendicular line positions and by matching the simulated line shape against the experimental spectrum. In particular, the symmetric shape and the unusually high relative intensity of the Zn:$M_I = -3/2$ perpendicular doublet are quite sensitive to changes in $A_\parallel$. This fortunate circumstance

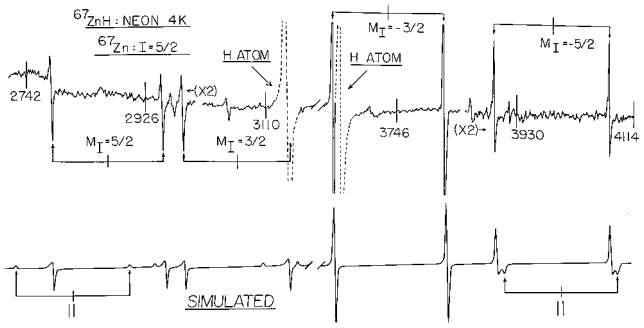

Figure 5. Four of the six M_I components for ^{67}Zn ($I = {}^5/_2$) are labeled for each hydrogen hyperfine doublet of the ^{67}ZnH radical in this neon-matrix ESR spectrum. Vertical scale changes are denoted by "×2", and the magnetic field corresponding to g_e occurs at 3418 G. Dashed lines mark the H atom doublet absorptions. The experimental spectrum is compared with a simulated ESR spectrum of ^{67}ZnH in the lower trace. The weak parallel (||) absorption features for the lowest- and highest-field hydrogen doublets are labeled accordingly. Note the unusually high intensity and symmetric nature of the ^{67}Zn:$M_I = -{}^3/_2$ hydrogen doublet, which occurs because of coincidence in line positions between the parallel (||) and perpendicular (⊥) lines for this particular ^{67}Zn hyperfine feature.

arises from the coincidence of the parallel and perpendicular line positions for this ^{67}Zn:$M_I = -{}^3/_2$ hyperfine component. The simulated spectrum of ^{67}ZnH in Figure 5 shows the low relative intensity of the parallel absorption features.

C. Theoretical Results. As part of this experimental study of the CH_3Zn and ZnH radicals, theoretical ab initio calculations were also performed. The CH_3Zn geometry was evaluated in C_{3v} symmetry with Gaussian 94[64] at the full second-order Møller−Plesset (MP2) level, using the uncontracted Wachters basis set[68] with the two additional recommended p functions for zinc (14s 11p 5d) and the uncontracted Dunning DZP sets[69] for carbon (9s 5p 1d) and hydrogen (4s 1p). The following values were obtained for the optimized geometry: $R_{Zn-C} = 1.982$ Å, $R_{C-H} = 1.088$ Å, and ∠H−C−Zn = 110.8°. This geometry agrees reasonably well with that obtained experimentally by Barckholtz and co-workers[5] from the ZEKE spectrum of CH_3Zn in its X^2A_1 state which, assuming $R_{C-H} = 1.1$ Å, gives $R_{Zn-C} = 2.001$ Å and ∠H−C−Zn = 109.7°. Barckholtz and co-workers also reported the geometry and vibrational frequencies calculated with density functional theory. There are several earlier reports of SCF and MP2 ab initio calculations of the geometry of the CH_3Zn radical.[2−4] Jamorski and co-workers[3] reported a geometry of $R_{Zn-C} = 1.987$ Å, $R_{C-H} = 1.094$ Å, and ∠H−C−Zn = 111.0°, obtained using an MP2 calculation with a contracted version of a basis set very similar to that which we have used. They also reported a geometry of $R_{Zn-C} = 2.094$ Å, $R_{C-H} = 1.090$ Å, and ∠H−C−Zn = 107.4°, obtained using an MP2 calculation with a valence double-ζ effective core potential (ECP) basis set incorporating d-type polarization functions for zinc and carbon.[4]

The hyperfine coupling constants for CH_3Zn were obtained from Hartree−Fock singles and doubles configuration interaction (HFSDCI) and multireference singles and doubles configuration interaction (MRSDCI) calculations using the MELDF suite of programs.[63] The same basis sets as discussed above were employed. The HFSDCI calculations included all single excitations from the Hartree−Fock configuration and those doublet excitations with an energy contribution exceeding a threshold energy of 5×10^{-8} hartree. The MRSDCI calculation used 20 reference configurations, chosen on the basis of the CI-coefficient contribution to the aforementioned HFSDCI calculation, as the reference space for the CI calculation. These theoretically derived hyperfine coupling constants for the CH_3-Zn radical are presented, along with the experimental results, in Table 3.

TABLE 3: Comparison of the Experimental and Theoretical Magnetic Parameters (MHz) of the CH_3Zn Radical

	^{67}Zn		^{13}C		H	
	A_{iso}	A_{dip}	A_{iso}	A_{dip}	A_{iso}	A_{dip}
experimental[a]	569(3)	20(4)	182(19)	14(22)	−14(1)	−[b]
theoretical[c]						
HFSDCI[d,e]	536	19	85	10	−0.90	[−0.9, −5.8, 6.7]
MRSDCI[f]	514	18	93	12	−0.52	[−0.9, −6.4, 7.3]
DFT[g]	445	−	167	−	−8.6	−

[a] Experimental magnetic parameters (MHz) for a neon-matrix sample at 9.0 K. [b] Approximately zero. See text. [c] The Wachters uncontracted basis set for zinc with the recommended two additional p functions (14s 11p 5d)[68] and the uncontracted Dunning DZP sets for carbon (9s 5p 1d) and hydrogen (4s 1p)[69] were used. [d] All single excitations from the Hartree−Fock solution and those double excitations that exceeded an energy threshold of 5×10^{-8} hartree were retained in the CI calculation. [e] The HFSDCI calculation included 292 586 spin-adapted configurations, had a sum of squares of the coefficients in the reference space of 0.93, and had a total CI energy of −1818.2907 hartree. [f] The MRSDCI calculation used 20 reference configurations chosen on the basis of their CI coefficient from the HFSDCI calculation. The MRSDCI calculation included 788 108 spin-adapted configurations, had a sum of squares of the coefficients in the reference space of 0.93, and had a total CI energy of −1818.3007 hartree. All single excitations from the reference space and those double excitations that exceeded an energy threshold of 5×10^{-8} hartree were retained in the CI calculation. [g] DFT method used the same basis set as above.

Analogous calculations of the hyperfine coupling constants were performed for the ZnH radical, except that a threshold energy of 5×10^{-7} hartree was used for the HFSDCI calculation and 40 reference configurations were possible for the MRSDCI calculation. The gas-phase value of $R_{Zn-H} = 1.5944$ Å was used.[47] The results of these calculations are presented, along with the experimental results from the neon-matrix experiments for the ^{67}ZnH radical, in Table 2.

IV. Discussion

A. Comparison between Theoretical and Experimental Results. Table 3 shows the comparison between experimental neon-matrix ESR hyperfine coupling constants for the CH_3Zn radical and the theoretical results from the HFSCDI and MRSDCI calculations discussed above. The values of A_{iso} and A_{dip} were calculated from the experimental ESR ($A_\perp$ and $A_{||}$) values using standard expressions. For carbon and zinc, these values include corrections for $L\cdot I$ effects, which are small in this case because $g_\perp$ does not differ greatly from g_e.[62] The defining equations for A_{iso} and A_{dip} are the following:

$$A_{dip} = g_e g_n \beta_e \beta_n \langle (3\cos^2\Theta - 1)/2r^3 \rangle$$

$$A_{iso} = 8\pi g_e g_n \beta_e \beta_n |\psi(0)|^2/3$$

Because of the large uncertainty associated with the estimation of $A_{||}$ from the ^{13}C perpendicular splitting, the uncertainty in $A_{dip}(^{13}C)$ is approximately 160%. The A values derived from both of the observed trapping sites are equal within experimental error.

The agreement with experiment for both calculations is reasonable for the hyperfine properties of zinc. The value of $A_{dip}(^{67}Zn)$ agrees within the experimental uncertainty, and the value of $A_{iso}(^{67}Zn)$ is low by 5% for the HFSDCI and 9% for the MRSDCI calculation. The calculated hydrogen A_{iso} values (−0.9 and −0.5 MHz) are below the experimental value of

−14(1) MHz. (These experimental measurements cannot determine the sign of A_{iso}, but a negative assignment is consistent with the theoretical calculations.) However, an exact comparison is complicated by the fact that the hydrogen nuclei do not lie on the 3-fold axis, whereas the experimental value observed is the projection onto this axis frame. Also, the dipolar parts of the coupling-constant matrices are averaged by motion about the 3-fold axis, whereas the theoretical values are calculated values in the local magnetic frame for the hydrogen nuclei. It is interesting that a DFT calculation yields an A_{iso} value for H of −14.2 MHz using a fully uncontracted 6-311G** basis and a value of −8.6 MHz using the same basis that we employed for the MRSDCI calculation. The improved agreement with experiment using the DFT method indicates that the CI approach was apparently not including the correct amount of mixing between the three configurations, namely $Zn(4s^2)\,\dot{C}H_3$, Zn(sp)-CH_3, and $Zn^+CH_3^-$. For $A_{iso}(^{13}C)$, even at the lower bound set by the experimental uncertainty, the calculated MRSDCI value is low by about 50%. The DFT method also produces better agreement for this ^{13}C property, with a predicted value of 228 MHz using the 6-311G** basis and 167 MHz using the same basis as was used in our MRSDCI calculations.

The comparison between the experimental and theoretical hyperfine parameters for ZnH is given in Table 2. As with CH_3-Zn, excellent agreement is observed for the theoretical values of $A_{iso}(^{67}Zn)$ and $A_{dip}(^{67}Zn)$. The value of $A_{dip}(^{67}Zn)$ agrees within the experimental uncertainty, and the value of $A_{iso}(^{67}Zn)$ is low by about 4% for the HFSDCI and by about 6% for the MRSDCI calculation. The MRSDCI value for $A_{iso}(H)$ is closer to the experimental value than the HFSDCI value, but both are approximately 60% lower than the experimental value. The DFT(B3PW91) method (6-311G**) yields an $A_{iso}(^{67}Zn)$ value that is below experiment by 37%, but it produces an $A_{iso}(H)$ value of 598 MHz, which is much closer to experiment than that of the MRSDCI calculation. (See also Table 2.) The value of $A_{dip}(H)$ is expected to be close to zero, and this expectation is borne out by the small calculated value. These comparisons are again similar to our findings from an analogous comparison of the CdH and CH_3Cd radicals.[6]

B. Bonding in the CH_3Zn and ZnH Radicals. A linear combination of atomic orbitals-molecular orbital (LCAO-MO) model of the highest-occupied molecular orbital (HOMO) of the CH_3Zn radical is represented as follows:

$$\Psi(X^2A_1) = a_1\chi(\text{Zn 4s}) + a_2\chi(\text{Zn 4p}_z) + a_3\chi(\text{C 2s}) + a_4\chi(\text{C 2p}_z) + a_5\chi(\text{H 1s})$$

where $\Psi(X^2A_1)$ represents the molecular wave function of the HOMO, χ(Zn 4s) etc. represent the atomic orbitals, and a_1 etc. represent the coefficients of each atomic orbital involved in the combination. For ZnH, the χ(C 2s) and χ(C $2p_z$) orbitals are removed. The free atom comparison method (FACM) provides for the squares of these coefficients to be estimated by comparison of the experimental values of A_{iso} and A_{dip} with their atomic counterparts.

Atomic parameters from a commonly employed compilation were used for carbon and hydrogen to calculate these orbital coefficients.[62] For zinc, the value for A_{iso} is available;[62] however, the listed value for A_{dip} refers to that for an unpaired electron occupying the 3d atomic orbital. Therefore, it was necessary to evaluate an atomic value of A_{dip} for zinc for an unpaired electron occupying the 4p orbital to analyze our results. The hyperfine coupling constants a_s, $a_{1/2}$, and $a_{3/2}$ have been derived from level-crossing experiments involving emission from the excited $^3P_1$ and $^1P_1$ states of ^{67}Zn atoms in the gas phase by Landman and Novick.[70] The parameter a_s is equivalent to the atomic value of A_{iso},[71] and the atomic value of A_{dip} can be derived from $a_{1/2}$ and $a_{3/2}$ using the following relations, as reported by Ammeter and Schlosnagle:[71]

$$\bar{P} = {}^5/_{16}(a_{1/2} + a_{3/2})$$

$$A_{dip} = {}^2/_5\bar{P}$$

The zinc atomic values that were obtained are 1992 MHz for A_{iso} and 36 MHz for A_{dip}. For comparison, a commonly listed theoretical value of A_{iso} is 2087 MHz.[62]

The spin densities derived from this FACM analysis for the CH_3Zn and ZnH radicals are shown in Table 4, together with spin-density results from a Mulliken gross spin population analysis (MSPA) on the MRSDCI wave functions discussed above. Also shown in Table 4 are the equivalent spin-density results for the CH_3Cd[6] and CdH[7] radicals. For comparison, we have evaluated the cadmium spin densities using atomic parameters derived, as discussed above for zinc, from the gas-phase level-crossing experiments of Thadeus and Novick[72] on emission from the excited $^3P_1$ and $^1P_1$ states of ^{111}Cd atoms; the results are −12354 MHz for A_{iso} and −253 MHz for A_{dip}. These parameters yield values of a_2 that are almost double the earlier estimates for the analogous cadmium radicals.[6] However, for a direct comparison with the CH_3Zn and ZnH results, it seems appropriate to use a consistently derived set of atomic parameters. It should also be noted that the larger size of the relativistic effects expected for cadmium (compared with zinc) may not be negligible.

It is clear from Table 4 that the experimentally derived spin densities for CH_3Zn and CH_3Cd are very similar. The total (unscaled) spin density on the metal is 85% for CH_3Zn and 71% for CH_3Cd. A comparison of the total spin density on the

TABLE 4: Comparison of the Experimental and Theoretical Spin Densities for the CH_3Zn, CH_3Cd, ZnH, and CdH Radicals

	$^{67}Zn/^{111}Cd$		^{13}C		H	total
	$a_1^2\chi$(ns)	$a_2^2\chi(np_z)$	$a_3^2\chi$(2s)	$a_4^2\chi(2p_z)$	$a_5^2\chi$(1s)	$\sum_{i=1}^{5} a_i^2$
CH_3Zn[a]						
experimental[b]	0.29	0.56	0.05	0.13	−0.01	1.00
MRSDCI[a,c]	0.54	0.27[d]	0.03	0.11[e]	≈0	0.95
CH_3Cd[f]						
experimental[g]	0.26	0.45	0.05	0.16	−0.01	0.89
MRSDCI[h]	0.46	0.28	0.04	0.17	≈0	0.95
ZnH[a]						
experimental[b]	0.32	0.53	−	−	0.35	1.2
MRSDCI[a,i]	0.49	0.33[j]	−	−	0.15	0.97
CdH[f]						
experimental[g]	0.33	0.44	−	−	0.36	1.1
MRSDCI[h]	0.42	0.33	−	−	0.22	0.97

[a] This work. [b] The experimental values are calculated using the free atom comparison method (FACM). [c] Gross spin populations from the MRSDCI calculation with 20 reference configurations and a threshold for retaining double excitations in the CI of 5×10^{-8} hartree. [d] This is the gross spin population for the zinc $\chi(4p_z)$. The $\chi(4p_x)$ and $\chi(4p_y)$ values are 0.0005. [e] This is the gross spin population for the carbon $\chi(2p_z)$. The $\chi(2p_x)$ and $\chi(2p_y)$ values are 0.0022. [f] From ref 6. [g] The experimental values were determined by a FACM analysis of the magnetic parameters in ref 6, using the atomic A_{iso} and A_{dip} values derived from gas-phase level-crossing experiments.[72] See text. [h] Gross spin populations from a MRSDCI calculation in ref 6. [i] Gross spin populations from the MRSDCI calculation with 40 reference configurations and a threshold for retaining double excitations in the CI of 5×10^{-7} hartree. [j] This is the gross spin population for the zinc $\chi(4p_z)$. The $\chi(4p_x)$ and $\chi(4p_y)$ values are 0.0001.

carbon is complicated by the large experimental uncertainty involved in deriving $A_{dip}(^{13}C)$. Therefore, it is better to make a direct comparison of the ^{13}C $A_\perp$ values for both radicals, which are 166(3) MHz for $^{13}CH_3Zn$ and 163(3) MHz for $^{13}CH_3Cd$.[6] This result shows again the similarity between these radicals, although the ^{13}C $A_\perp$ comparison does assume that the carbon hybridization is the same for both radicals. This assumption seems reasonable, given that $A_{iso}(H)$, which is expected to be sensitive to changes in the metal−carbon−hydrogen bond angle, is very similar in the CH_3Zn and CH_3Cd radicals, with values of 14(1) and 17(1) MHz, respectively. Therefore, the carbon hybridization is also likely to be similar.

The experimentally derived spin densities for ZnH and CdH show the same behavior. The majority of the spin density is on the metal, with values of 74% for the ZnH radical and 77% for CdH. The hydrogen 1s characters are also equivalent for these two metal hydrides at about 35%. In a comparison of the two hydrides with the two methides, the total spin densities on the metals are equal within the experimental uncertainty and the inherent uncertainty in the FACM approximation.

The MSPA results show an interesting trend. For all radicals, the predicted metal s character is double, and the p character is almost half, the corresponding value obtained from the FACM analysis. Also, for these radicals, the MSPA results would indicate a slight shift to s character from p character for the zinc radical when compared with the corresponding cadmium radical. Given the experimental uncertainties involved in evaluating $A_{dip}(^{13}C)$, no comparison is made for the ^{13}C densities calculated; however, for the ZnH and CdH radicals, the calculated hydrogen s character is about half that predicted by the FACM analysis.

Barckholtz and co-workers have recently reported an "experimental" molecular-orbital (MO) diagram for CH_3Mg and CH_3Zn.[5] This MO diagram was derived from ZEKE-PFI spectroscopic measurements. The bonding in CH_3Zn is described by a $\sigma^2\sigma^{*1}$ configuration, where the σ and σ^* orbitals are formed from the overlap of the zinc atomic 4s orbital and the sp^3 hybrid HOMO of the methyl group. Such a picture appears to be inconsistent with our results, as we show a significant amount of Zn 4p character in the HOMO of this radical, in the range of 50%. The MO description, given by Jackson, of the two σ orbitals being formed from the overlap of the sp^3 hydrid HOMO of the methyl group and an sp hybrid formed by the linear combination of the zinc atomic 4s and $4p_z$ orbitals would seem more consistent with our results.[18] The doubly occupied lower-energy σ orbital would be expected to have larger zinc 4s character at the expense of the singly occupied σ^* orbital, which would, in turn, have higher 4p character.

It is interesting to note that the metal carbon bond dissociation energy for the CH_3Zn radical [25(4) kcal/mol] is higher than that of the CH_3Cd radical [15(3) kcal/mol].[10] The higher stability of the CH_3Zn radical could explain why we observe higher yields of the CH_3Zn radical compared to CH_3Cd under similar generation and deposition conditions.

Barckholtz and co-workers[5] also derived the MO diagram for $(CH_3)_2Zn$ using the MO diagram they had derived for CH_3Zn. This MO diagram predicts that the radical cation of $(CH_3)_2Zn$ would have a HOMO composed of the overlap of the zinc atomic 4s orbital and the HOMOs of the two methyl groups. We have recorded the ESR spectrum[73] of $(CH_3)_2Zn^+$ in neon matrixes, and it is not consistent with this picture. Instead, the HOMO is completely dominated by zinc 4p character.

C. Analysis of the *g* Tensor of the CH_3Zn and ZnH Radicals. Additional evidence showing the similarity in the electronic structures of CH_3Zn and ZnH is provided by the following analysis of their *g* tensors, which indicates nearly identical amounts of metal $4p_z$ character. The $g_\perp$ value for the CH_3Zn radical is smaller than the g_e value, giving a $\Delta g_\perp$ value of −0.0188(5), where $\Delta g_\perp = g_\perp - g_e$. This deviation can be expressed by the approximate relationship $\Delta g_\perp = -2\zeta_{4p}a_2^2/\Delta E$, where ζ_{4p} is the metal spin−orbit parameter (385 cm^{-1} for zinc[74]), a_2^2 is the 4pσ character of the HOMO, and ΔE is the energy separation between the ground state and the excited ^2E state.[75] Using a value for $\Delta E(A^2E_{1/2}\leftarrow X^2A_\perp)$ of 23 950 cm^{-1},[22] a_2^2 is calculated from the experimental value of $\Delta g_\perp$ to be 0.58. As discussed above, the FACM analysis of the zinc A_{dip} value for the CH_3 Zn radical yields an a_2^2 value of 0.56. The analogous calculation performed for ZnH, using a value for $\Delta E(A^2\Pi\leftarrow X^2\Sigma)$ of 23 280 cm^{-1}, [47] yields an a_2^2 result of 0.54, based on the neon experimental value of $\Delta g_\perp = 0.0182$. Analogous calculations for the CH_3Cd and CdH radicals yielded a_2^2 values of 0.51 and 0.50, respectively.

V. Summary

Various isotopomers of the CH_3Zn radical have been isolated in a neon matrix and studied for the first time by ESR spectroscopy. The radicals were formed by the reaction of laser-ablated zinc with various methyl precursors. The ^{67}Zn, ^{13}C, and D isotopomers of CH_3Zn were all generated. Values for $g_\perp$, $A_{iso}(^{67}Zn)$, $A_{iso}(H)$, $A_{iso}(D)$, $A_{iso}(^{13}C)$, $A_{dip}(^{67}Zn)$, and $A_{dip}(^{13}C)$ were derived for the CH_3Zn radical from these matrix ESR spectral results. The first measurements of the metal hyperfine structure in ^{67}ZnH, formed from the reaction of laser-ablated zinc with hydrogen gas, have been reported and fully interpreted.

Ab initio calculations were performed on the CH_3Zn and ZnH radicals. The MP2-level geometry derived for the CH_3Zn radical was consistent with the recently reported gas-phase value.[5] HFSDCI and MRSDCI calculations of the nuclear hyperfine coupling constants for both radicals showed reasonable agreement with the experimental values. The calculated ^{67}Zn hyperfine parameters, $A_{iso}(^{67}Zn)$ and $A_{dip}(^{67}Zn)$, agreed within 10% for both the CH_3Zn and the ZnH radicals. The calculated value of $A_{iso}(^{13}C)$ for the CH_3Zn radical was low by 50%, and that of $A_{iso}(H)$ for the ZnH radical was low by 60%, when the MRSDCI method was employed. With DFT, better agreement was achieved for H and ^{13}C, but poorer agreement was found for the metal A_{iso} values. The free atom comparison method was employed to estimate the atomic orbital characters of the HOMO for the CH_3Zn and ZnH radicals. This analysis showed that the HOMOs of both radicals were very similar and were composed of about 30% Zn 4s character and 50% Zn 4p character. An analysis of the spin−orbit coupling contribution to the *g* shift also yielded a value of about 50% for the Zn 4p character in both radicals. This analysis was compared with a Mulliken gross spin population analysis (MSPA) of the MRSDCI wave function, which showed a similar total spin density on the metal but a lower Zn 4p character of approximately 30% for both radicals. Comparisons of the CH_3Zn and ZnH radicals with their cadmium analogues showed the bonding in all four radicals to be quite similar.

Acknowledgment. The authors express their appreciation to Professor E. R. Davidson (Indiana University, Bloomington, IN) for the DFT calculations of A_{iso} and for his help in analyzing why the CI calculations yielded A_{iso} values that differed substantially from the experimental results. A.J.M. thanks the Australian Research Council for support of this work under the Small Grants Scheme, The Australian Government Department

of Education, Employment, Training and Youth affairs (DEETYA), who provided a Research Infrastructure, Equipment and Facilities Grant that was used to purchase the ESR spectrometer at UWA. E.K. also thanks DEETYA for providing him with an Australian Postgraduate Award with stipend. E.K. also expresses his appreciation to UWA for granting him a Jean Rogerson Postgraduate Scholarship. A.J.M. and E.K. thank the Technicians of the Chemistry Workshop for their continuing assistance and support. Appreciation is expressed to Dr. David Feller and Professor E. R. Davidson for use of their MELDF program for calculating the nuclear hyperfine parameters. Support from the National Science Foundation (CHE-9319291) and a Research Corporation Cottrell College Science Award is gratefully acknowledged (L.B.K.), as is undergraduate research support from an NSF REU site grant to Furman University. Drs. Knight and McKinley express their appreciation to the Camille and Henry Dreyfus Foundation for an earlier Scholar-Fellow Award that initially established these collaborative investigations.

References and Notes

(1) Knight, L. B., Jr.; Weltner, W., Jr. *J. Chem. Phys*. **1971**, *55*, 2061.
(2) Kaupp, M.; Stoll, H.; Preuss, H. *J. Comput. Chem*. **1990**, *9*, 1029.
(3) Jamorski, C.; Dargelos, A. *Chem. Phys.* **1992**, *164*, 191.
(4) Jamorski, C.; Dargelos, A.; Teichteil, Ch.; Daudey, J. P. *Chem. Phys.* **1993**, *178*, 39.
(5) Barckholtz, T. A.; Powers, D. E.; Miller, T. A.; Bursten, B. E. *J. Am. Chem. Soc*. **1999**, *121*, 2576.
(6) Karakyriakos, E.; Davis, J. R.; Wilson, C. J.; Yates, S. A.; McKinley, A. J.; Knight, L. B., Jr.; Babb, R.; Tyler, D. J. *J. Chem. Phys.* **1999**, *110*, 3398.
(7) Knight, L. B., Jr.; Miller, P. K.; Steadman, J. *J. Chem. Phys*. **1984**, *80*, 4587.
(8) Young, P. J.; Gosavi, R. K.; Connor, J.; Strausz, O. P.; Gunning, H. E. *J. Chem. Phys.* **1973**, *58*, 5280.
(9) Yu, C. F.; Youngs, F.; Tsukiyama, K.; Bersohn, R. *J. Chem. Phys*. **1986**, *85*, 1382.
(10) Jackson, R. L. *Chem. Phys. Lett.* **1989**, *163*, 315.
(11) Kuech, T. F. *Mater. Sci. Rep.* **1987**, *2*, 1.
(12) Ruda, H. E. *Widegap II−VI Compounds for Opto-electronic Applications*; Chapman & Hall: London, 1992.
(13) Sigel, H. *Metal Ions in Biological Systems. Vol. 15: Zinc and Its Role in Biology and Nutrition*; Marcel Dekker: New York, 1983.
(14) See, for example: Watterich, A.; Gillam, O. R.; Kappers, L. A.; Raksanyi, K. *Solid State Commun*. **1996**, *97*, 477.
(15) See, for example: Felix, C. C.; Sealy, R. C. *J. Am. Chem. Soc*. **1981**, *103*, 2831.
(16) See, for example: *Selective Hydrocarbon Activation: Principles and Progress*; Davies, J. A., Watson, P. L., Greenberg, A., Liebman, J. F., Eds.; VCH Publishers: New York, 1990.
(17) Knochel, P. *Comprehensive Organic Synthesis*; Trost, B. M., Fleming, I., Eds.; Pergamon Press: Elmsford, NY, 1991; Vol. 1, p 212.
(18) Jackson, R. L. *Chem. Phys. Lett*. **1990**, *174*, 53.
(19) Robles, E. S. J.; Ellis, A. M.; Miller, T. A. *Chem. Phys. Lett*. **1991**, *178*, 185.
(20) Jackson, R. L. *J. Chem. Phys.* **1992**, *96*, 5938.
(21) Povey, I. M.; Bezant, A. J.; Corlett, G. K.; Ellis, A. M. *J. Phys. Chem*. **1994**, *98*, 10427.
(22) Cerny, T. M.; Tan, X. Q.; Williamson, J. M.; Robles, E. S. J.; Ellis, A. M.; Miller, T. A. *J. Chem. Phys*. **1993**, *99*, 9376.
(23) Hauge, R. H.; Margrave, J. L.; Kafafi, Z. H. *Chemistry and Physics of Matrix Isolated Species*; Andrews, L., Moskovits, M., Eds.; North-Holland: Amsterdam, 1989.
(24) Bai, H.; Ault, B. S. *J. Phys. Chem*. **1994**, *98*, 6082.
(25) Bai, H.; Ault, B. S. *J. Phys. Chem*. **1994**, *98*, 10001.
(26) Bai, H.; Ault, B. S. *J. Phys. Chem*. **1995**, *99*, 10492.
(27) Greene, T. M.; Andrews, L.; Downs, A. J. *J. Am. Chem. Soc*. **1995**, *117*, 8180.
(28) Greene, T. M.; Brown, W.; Andrews, L.; Downs, A. J.; Chertihin, G. V.; Runeberg, N.; Pyykkõ, P. *J. Phys. Chem*. **1995**, *99*, 7925.
(29) Bracken, V. A.; Gürtler, P.; McCaffrey, J. G. *J. Phys. Chem. A* **1997**, *101*, 9854.
(30) Bracken, V. A.; Legay-Sommaire, N.; McCaffrey, J. G. *J. Phys. Chem. A* **1997**, *101*, 9863.
(31) Knight, L. B., Jr.; Herlong, J. O.; Cobranchi, S. T.; Kirk, T. *J. Chem. Phys.* **1990**, *92*, 6463.
(32) Knight, L. B., Jr.; Cobranchi, S. T.; Petty, J.; Cobranchi, D. P. *J. Chem. Phys.* **1989**, *91*, 4587.
(33) Ozin, G. A.; McCaffrey, J. G.; Parnis, J. M. *Angew. Chem., Int. Ed. Engl*. **1986**, *25*, 1072.
(34) Knight, L. B., Jr.; Banisaukas, J. J., III; Babb, R.; Davidson, E. R. *J. Chem. Phys.* **1996**, *105*, 6607.
(35) Parnis, J. M.; Ozin, G. A. *J. Phys. Chem*. **1989**, *93*, 1204.
(36) Xin, J.; Robinson, J. S.; Apponi, A. J.; Ziurys, L. M. *J. Chem. Phys*. **1998**, *108*, 2703.
(37) Brazier, C. R.; Bernath, P. F. *J. Chem. Phys.* **1989**, *91*, 4548.
(38) Marr, A. J.; Grieman, F.; Steimle, T. C. *J. Chem. Phys.* **1996**, *105*, 3930.
(39) Anderson, M. A.; Ziurys, L. M. *Astrophys. J.* **1996**, *460*, L77.
(40) Rubino, R.; Williamson, J. M.; Miller, T. A. *J. Chem. Phys.* **1995**, *103*, 5964.
(41) Anderson, M. A.; Ziurys, L. M. *Astrophys. J.* **1995**, *452*, L157.
(42) Li, B.-Z.; Xin, J.; Ziurys, L. M. *Chem. Phys. Lett*. **1997**, *280*, 513.
(43) Anderson, M. A.; Robinson, J. S.; Ziurys, L. M. *Chem. Phys. Lett*. **1996**, *257*, 471.
(44) Brazier, C. R.; Bernath, P. F. *J. Chem. Phys.* **1986**, *86*, 5918.
(45) Tan, X. Q.; Cerney, T. M.; Williamson, J. M.; Miller, T. A. *J. Chem. Phys.* **1994**, *101*, 6396.
(46) Panov, S. I.; Powers, D. E.; Miller, T. A. *J. Chem. Phys.* **1998**, *108*, 1335.
(47) Huber, K. P.; Herzberg, G. *Molecular Spectra and Molecular Structure. IV. Constants of Diatomic Molecules*; Van Nostrand Reinhold: New York, 1979.
(48) Wojslaw, R. S.; Perry, B. F., Jr. *Astrophys. J., Suppl. Ser.* **1976**, *31*, 75.
(49) Perry, B. F., Jr. *Publ. Astron. Soc. Jpn.* **1979**, *31*, 461.
(50) Dufayard, J.; Nedelec, O. *J. Phys.* **1977**, *38*, 449.
(51) Kedzierski, W.; Supronowicz, J.; Atkinson, J. B.; Krause, L. *Can. J. Phys*. **1990**, *68*, 526.
(52) Urban, R.-D.; Magg, U.; Birk, H.; Jones, H. *J. Chem. Phys*. **1990**, *92*, 14.
(53) Birk, H.; Urban, R.-D.; Polomsky, P.; Jones, H. *J. Chem. Phys*. **1991**, *94*, 5435.
(54) O'Brien, L. C.; Fernando, W. T. M. L.; Bernath, P. F. *J. Mol. Spectrosc*. **1990**, *139*, 424.
(55) Goto, M.; Namiki, K.; Saito, S. *J. Mol. Spectrosc*. **1995**, *173*, 585.
(56) Tezcan, F. A.; Varberg, T. D.; Stroh, F.; Evenson, K. M. *J. Mol. Spectrosc*. **1997**, *185*, 290.
(57) Breckenridge, W. H. *J. Phys. Chem*. **1996**, *100*, 14840.
(58) Jamorski, C.; Dargelos, A.; Teichteil, Ch.; Daudey, J. P. *J. Chem. Phys*. **1994**, *100*, 917.
(59) Salazar, M. R.; Simons, J. *J. Chem. Phys.* **1999**, *110*, 229.
(60) Knight, L. B., Jr.; Steadman, J.; Miller, P. K.; Cleveland, J. A., Jr. *J. Chem. Phys.* **1988**, *88*, 2226. Knight, L. B., Jr.; Kaup, J. G.; Petzoldt, B.; Ayyad, R.; Ghantz, T. K.; Davidson, E. R. *J. Chem. Phys.* **1999**, *110*, 5658.
(61) Knight, L. B., Jr.; Cobranchi, S. T.; Earl, E. *J. Chem. Phys*. **1988**, *88*, 7348.
(62) Weltner, W., Jr. *Magnetic Atoms and Molecules*; Van Nostrand Reinhold: New York, 1983.
(63) MELDF was originally written by L. McMurchie, S. Elbert, S. Langoff, and E. R. Davidson. It has been substantially modified by D. Feller, R. Cave, D. Rawlings, R. Frey, R. Daasch, L. Mitzche, P. Phillips, K. Iberle, C. Jackels, and E. R. Davidson.
(64) Frisch, M. J.; Trucks, G. W.; Schlegel, H. B.; Gill, P. M. W.; Johnson, B. G.; Robb, M. A.; Cheeseman, J. R.; Kieth, T.; Petersson, G. A.; Montgomery, J. A.; Raghavachari, K.; Al-Laham, M. A.; Zakrzewski, V. G.; Ortiz, J. V.; Foresman, J. B.; Cioslowski, J.; Stefanov, B. B.; Nanayakkara, A.; Challacombe, M.; Peng, C. Y.; Ayala, P. Y.; Chen, W.; Wong, M. W.; Andres, J. L.; Replogle, E. S.; Gomperts, R.; Martin, R. L.; Fox, D. J.; Binkley, J. S.; Defrees, D. J.; Baker, J.; Stewart, J. P.; Head-Gordon, M.; Gonzalez, C.; Pople, J. A. *Gaussian 94*, revision D.2; Gaussian, Inc.: Pittsburgh, PA, 1995.
(65) Kasai, P. H.; Whipple, E. B. *J. Am. Chem. Soc.* **1967**, *89*, 1033.
(66) Knight, L. B., Jr.; Steadman, J.; Feller, D.; Davidson, E. R. *J. Am. Chem. Soc*. **1984**, *106*, 3700.
(67) Knight, L. B., Jr.; Steadman, J. *J. Chem. Phys*. **1983**, *78*, 5940.
(68) Wachters, A. J. H. *J. Chem. Phys*. **1970**, *52*, 1033.
(69) Dunning, T. H., Jr.; Hay, P. J. *Methods of Electronic Structure Theory*; Schaefer, H. F., III, Ed.; Plenum Press: New York, 1977; Vol. 2.
(70) Landman, A.; Novick, R. *Phys. Rev.* **1964**, *134*, A56.
(71) Ammeter, J. H.; Schlosnagle, D. C. *J. Chem. Phys.* **1973**, *59*, 4784.
(72) Thaddeus, P.; Novick, R. *Phys. Rev.* **1962**, *126*, 1774.
(73) Knight, L. B., Jr.; McKinley, A. J. In preparation.
(74) Sugar, J.; Musgrove, A. *J. Phys. Chem. Ref. Data* **1995**, *24*, 1803.
(75) Knight, L. B., Jr.; Lin, K. C. *J. Chem. Phys*. **1972**, *56*, 6044.